Ligand-induced self-assembly of twisted two-dimensional halide perovskites

Jonghee Yang[1], Addis S. Fuhr[2], Kevin M. Roccapriore[2], Bogdan Dryzhakov[2,3], Bin Hu[3], Bobby G. Sumpter[2], Sergei V. Kalinin[3,4], Mahshid Ahmadi[3]*

[1] Department of Chemistry, Yonsei University, Seoul 03722, Republic of Korea.

[2] Center for Nanophase Materials Sciences, Oak Ridge National Laboratory, Oak Ridge, TN 37830, United States.

[3] Institute for Advanced Materials and Manufacturing, Department of Materials Science and Engineering, University of Tennessee, Knoxville, TN 37996, United States.

[4] Pacific Northwest National Laboratory, Richland, WA 99354, United States.

*Corresponding author e-mail: mahmadi3@utk.edu

Abstract

Two-dimensional (2D) halide perovskites (HPs) are now an emerging materials system that exhibits intriguing optoelectronic functionalities. Conventionally, they have been synthesized with linear and/or planar molecular spacers, rendering nominal modifications in optoelectronic properties. In contrast, lower dimensional HPs (0D and 1D) have been accommodating to the incorporation of bulky molecular spacers, leaving fundamental insights to remain elusive in their application for unconventional 2D HP structures. Herein, by implementing a high-throughput autonomous exploration workflow, crystallization behaviors of 2D HPs based on bulky 3,3-diphenylpropylammonium (DPA) spacer are comprehensively explored. Counterintuitive to the conventional HP chemistry, synthesis of 2D DPA_2PbI_4 HP is indeed feasible when the steric hindrance is mediated by minute incorporation of 3D HPs. Furthermore, a Moiré superlattice is observed from the DPA_2PbI_4 flakes, indicating the spontaneous formation of twisted stacks of 2D HPs – the first time to the best our knowledge. We hypothesize that the unconventional van der Waals surface of DPA_2PbI_4 facilitates the self-assembly of the twisted stacks of 2D HPs. This work exemplifies how high-throughput experimentation can discover unconventional material systems where the synthetic principle lies beyond the conventional chemical intuition. Furthermore, these findings provide hints on how to 'chemically' manipulate the twist stacking in 2D HPs, thus rendering a straightforward way for bespoke realization of functionalities in exotic materials systems via bottom-up approach.

Introduction

Two-dimensional (2D) halide perovskites (HPs) have become an emerging semiconductor platform because of their intriguing optoelectronic features originating from the distinctive structures/compositions as well as synthetic feasibility. The large organic cations, called spacers, confine the inorganic lattice – a $[BX_6]^{4-}$ octahedra (B and X are divalent metal cations and halides, respectively) as a unit cell – into a monolayer thickness as a Ruddlesden-Popper (RP) structure (chemical formula of L_2BX_4)[1]. The distinctive organic-inorganic hybrid structure, where the organic cations serve as a dielectric barrier, renders a quantum-well electronic structure manifesting in sharp and strong excitonic emissions that are not observed in 3D HP counterparts[1, 2]. The feasibility of synthesizing 2D HPs via solution processing at low temperatures presents significant advantages compared to conventional 2D materials that require energy-consuming synthetic conditions[3, 4]. These merits of 2D HPs open a new avenue for realizing the promising potential for future optoelectronic applications.

The optoelectronic properties of 2D HPs are largely dependent on the structural alignments and distortions of the inorganic octahedra, which are greatly influenced by the selection of spacer cations[5-7]. Specifically, the strong surface binding, as well as the intermolecular interaction along the spacer cations coordinated at the 2D HP surfaces can induce non-trivial strain to the inorganic lattices[7]. Such supramolecular interactions subsequently lead to the 'octahedral distortion', where the constituent atoms in the inorganic lattice are minutely off from the ideal positions, thereby involving appreciable changes in their electronic structures[5-7]. Furthermore, recent efforts have demonstrated the modification of quantum-well electronic structures by introducing semiconducting molecular spacers, subsequently realizing wide-range tuning of the 2D HP optoelectronic properties[8, 9]. Note that, given the structural, chemical, and electronic varieties in spacer cations, 2D HPs have infinite structural flexibility and thus tunability in their optoelectronic features[1, 10-13].

To date, various spacer cations with different sizes and shapes have been explored for 2D HP demonstration (particularly, for RP-type HPs), which typically have linear and/or planar molecular structures that are likely to form a well-ordered spacer alignment across the surfaces[1, 11, 13-15]. This, in turn, can render a smoothed and planar van der Waals surface of organic cations of 2D HP faces, thereby allowing a favorable construction of a coherent, epitaxial stack of inorganic lattice sheets. Thus in general, octahedral distortion in 2D HPs is insignificant when using conventional 2D spacers. As a result, there are nominal changes in electronic strucures, indicating the tunability of optoelectronic functionality is inherently limited[6, 7, 16, 17].

Intuition based on steric hindrance would indicate that the use of non-linear and bulky molecular spacers would induce a stronger strain to 2D HP inorganic lattice, as a result of the substantial steric hindrances between the neighboring molecules upon their compact packing at the HP surface. Subsequently, this would manifest as a larger magnitude of octahedral distortion in the 2D HP, thereby leading to distinctive changes in the electronic structures. Notwithstanding its significance for the bespoke realization of optoelectronic functionalities, such a strategy has never been considered. Consequently, fundamental insights into lattice formation (i.e., crystallization), structural ordering, and the resulting optoelectronic properties of 2D HPs based on bulky spacer cations remain elusive.

Herein, we explore the formation behaviors and optoelectronic features of a 2D HP system

3

employing a representative bulky spacer cation – 3,3-diphenylpropylammonium (DPA)[18] – via high-throughput autonomous experimentation[2, 15, 19-22]. Through combinatorial precursor mixing of 2D DPA_2PbI_4 with $APbI_3$ – A is cesium (Cs), methylammonium (MA), and formamidinium (FA) – and the subsequent crystallization, with support of theoretical calculations, it is found that minute incorporation of $APbI_3$ is vital for realization of 2D DPA_2PbI_4 HP crystallites. Compared with the conventional 2D HPs, the synthesized DPA_2PbI_4 exhibits a highly blueshifted PL with an asymmetric spectral shape irrespective of the A-site cations. To describe these observations, we hypothesize that such minute incorporation of the A-site cation into the corresponding vacancies can mediate the steric hindrance between the neighboring DPA cation upon the compact packing. As a result, this allows for feasible crystallization of the 2D DPA_2PbI_4 HP structure, but still involves substantially distorted inorganic $[BX_6]^{4-}$ octahedra attributed to the remnant strain induced by DPA. This leads to notable modifications in electronic structure and the consequent optoelectronic properties[7, 23].

The compact packing of bulky DPA upon coordination in 2D DPA_2PbI_4 HP can render an unconventional van der Waals interface in an HP sheet stack, which deviates from a planar feature in conventional 2D HPs employing the spacer cations with linear and/or planar molecular structures. Such an extraordinary electrostatic surface can manifest different layer-stacking modes upon thin-film crystallization compared with the conventional 2D HPs. Indeed, we observe the emergence of an atomic Moiré superlattice in a 2D DPA_2PbI_4 HP flake directly crystallized onto a substrate, with a twist angle of ~4° that is consistent with theoretical predictions. This indicates that, for the first time (to our best knowledge), a twisted stack of 2D HPs can be formed by employing the bulky DPA spacer. It should be noted that the twisted 2D HP stacks are spontaneously synthesized during crystallization without any top-down direction-manipulation process that is employed in typical 2D materials systems. This strongly suggests that our observation is exclusively driven by a straightforward self-assembly action, which is attributed to the delicate supramolecular interactions across the spacer cations at the 2D layer interface.

This work exemplifies how the high-throughput autonomous exploration workflow can discover new unconventional material systems and their functionalities in an accelerated way, where the corresponding synthetic principle lies beyond conventional chemical intuition. Also, our findings present fresh insight into the 'chemical' manipulation of the twist angles in 2D HPs, thus establishing the design principles required for the construction of unconventional materials systems via – straightforward and cost-effective – bottom-up approach. Specifically, given that meticulous experimental procedure and extensive efforts are required for constructing twisted HP structure[24], this work demonstrate how judicious selection of spacer cations can easily synthesize such unconventional and intriguing structures. This, in turn, will initiate new explorations in unconventional optoelectronic behaviors, thereby accelerating discoveries of exotic functionalities in 2D HP systems.

Synthetic feasibility of DPA-based 2D HPs

It is known that conventional 2D HPs, employing spacer cations with linear and/or planar structures can be readily synthesized[1, 23]. While extensive efforts have been focused on the conventional 2D HPs[7, 8, 13-15], systems with a bulky spacer have not been explored. Such structures are hard to envisage due to substantial steric hindrance based on classical chemical

intuition. In our work we choose DPA – a ligand utilized for 3D perovskites (or nanocrystals) system[18] – as a representative bulky spacer cation, and explored its synthetic feasibility to form a 2D DPA_2PbI_4 structure. Two separate phenyl rings in the DPA molecular structure should bestow a large steric hindrance between the vicinal DPA cations upon their compact packing on 2D HP surfaces. In turn, this is likely to affect the structural stability, or synthetic feasibility of a complete DPA_2PbI_4 structure.
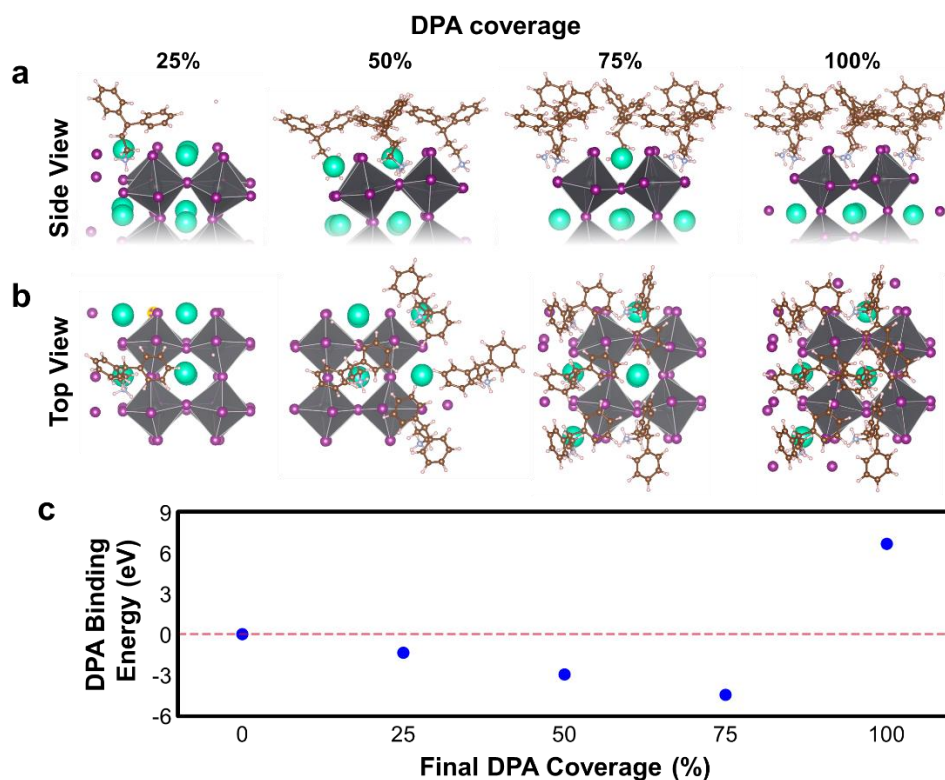

Figure 1. (**a**) Side and (**b**) top views of the optimized DPA-coordinated $CsPbI_3$ lattices with different DPA coverages. (**c**) Calculated binding energies of the DPA ligand on an A-cation vacancy at the $CsPbI_3$ surfaces with different DPA coverages.

To gain insight into the synthetic feasibility of the DPA_2PbI_4, we initially evaluated the impact of steric hindrance associated with DPA cations coordinated on the perovskite surface structure via Density Functional Theory (DFT) calculations. Here we varied the coverage ratios of DPA cation on the 3D $CsPbI_3$ perovskite surface – the lattice with a simplest A-site cation – from 25 to 100% (**Figure 1a and b**). From the respective optimized surface structures, it is observed that the arrangement of $[PbI_6]^{4-}$ octahedra becomes distorted with increasing DPA coverage ratios, suggesting that the perovskite lattice structure becomes unstable with increasing the density of surface-coordinated bulky DPA.

To further obtain quantitative insight into the feasibility of bulky DPA coordination on perovskite lattice as a function of its coverage ratios (i.e., densities), the binding energies of DPA as a ligand on a Cs vacancy at the perovskite lattice with different DPA coverages were calculated (**Figure 1c**, details of the DFT calculations are demonstrated in **Methods**). It is observed that the magnitude of the binding energy of a DPA cation on the $CsPbI_3$ surface gradually increased in the negative range with increasing surface DPA coverage ratios up to

5

75%, indicating feasible binding action of DPA on the surface. However, at higher magnitude of surface DPA coverage (100%), there is an abrupt change to a positive value. This indicates that the coordination of DPA cation onto A-site vacancy at the perovskite surface is unlikely feasible at 100% coverage condition. It is speculated that the steric hindrance between the neighboring bulky DPA cations at the surface not only causes an octahedral distortion in the HP lattice but also impedes the appropriate coordination of the ligand at this coverage ratio. With such distinctive octahedral distortion and unfeasibility of DPA coordination in the complete surface coverage, it is envisaged that the synthesis of pure DPA_2PbI_4, where DPA cations are fully covered on the A-site vacancy in n=1 2D HP, is likely not feasible. We note here that the exploration has been done on relatively small unit cell size mainly due to the large numbers of atoms in DPA cation, which limits the range of possible DPA coverage ratios to be explored by DFT. This implies that the maximum DPA coverage exceeds the calculated value of 75%, but would be lower than 100% in the real system.
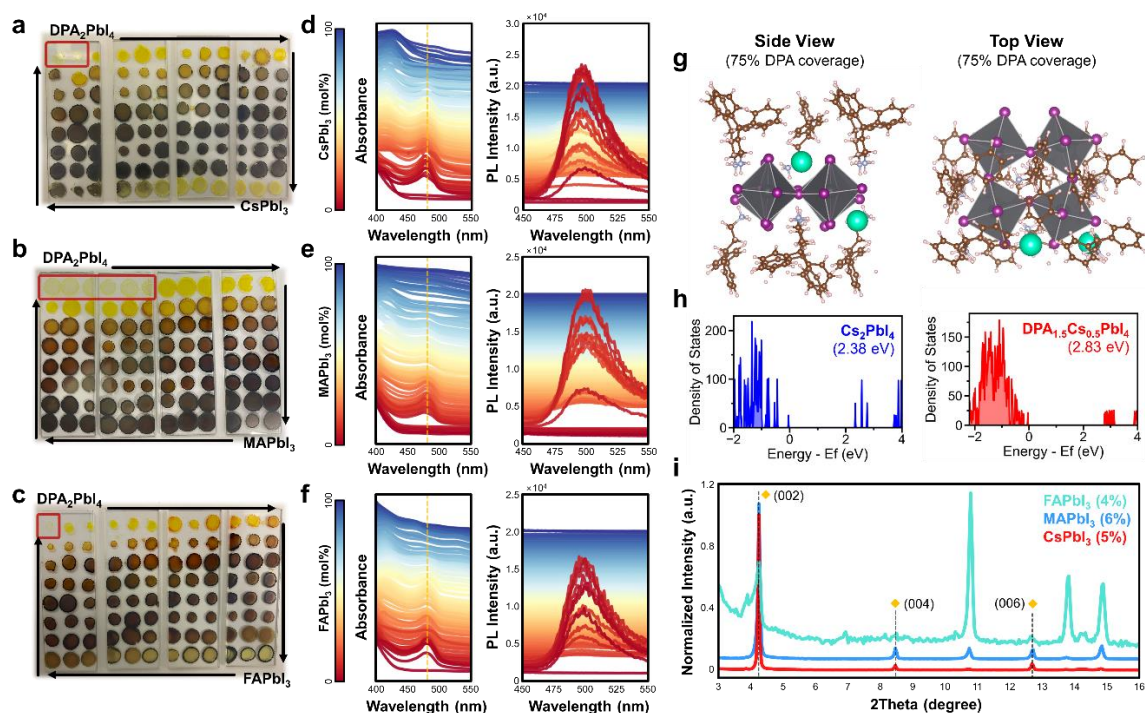
Figure 2. (**a-c**) High-throughput synthesized film arrays of DPA_2PbI_4-based quasi-2D HPs with (**a**) $CsPbI_3$, (**b**) $MAPbI_3$, and (**c**) $FAPbI_3$ endmembers, respectively. (**d-f**) Corresponding absorption and PL spectra of the DPA_2PbI_4-based quasi-2D HP film arrays with (**d**) $CsPbI_3$, (**e**) $MAPbI_3$, and (**f**) $FAPbI_3$ endmembers, respectively. (**g**) Side and top views of an optimized 2D $DPA_{1.5}Cs_{0.5}PbI_4$ HP structure (i.e., 75% DPA coverage). (**h**) DFT calculated density of states profiles of Cs_2PbI_4 (i.e., 0% DPA coverage) and $DPA_{1.5}Cs_{0.5}PbI_4$ HP structure. (**i**) Normalized XRD patterns of 2D DPA2PbI4 HP film synthesized with incorporation of minimal composition ratios of $CsPbI_3$ (5%), $MAPbI_3$ (6%), and $FAPbI_3$ (4%), respectively.

To experimentally confirm the universality of our DFT results in DPA_2PbI_4 synthesis – the necessity of minute A-site substitution with small cation – we employed the high-throughput automated experimental workflow for the synthesis of 2D:3D HP compositional space. By

6

drop-casting the precursor mixture with different ratios of stoichiometric 2D DPA_2PbI_4 and 3D $APbI_3$ (A = Cs^+, MA^+ and FA^+) endmembers, combinatorial libraries of DPA-based (quasi-)2D HP film arrays are synthesized (**Figure 2a-c**)[2, 15, 19, 20, 22].

In all cases, it is observed that the precursor droplets cannot be transformed to film crystallites upon thermal annealing at 2D-rich concentrations (i.e., 99%, 95%, and 100% of 2D DPA_2PbI_4 for Cs-, MA- and FA-based systems, respectively; marked with red squares). The inappreciable UV/Vis absorption and PL spectral features at the corresponding compositions, as shown in **Figure 2d-f**, corroborate this. With increasing 3D $APbI_3$ composition ratios up to ~10-15%, the precursor solutions start to crystallize to form yellow films. Given the emergence of distinctive excitonic absorption peak at ~480 nm (marked with yellow dashed lines) as well as asymmetric PL signal peaked at ~490 nm in the corresponding spectra, we speculate the crystalline phase to be DPA-based 2D HPs with n=1 layer thickness (*vide infra*).

Note that the position of absorption and PL peaks are appreciably blueshifted compared to those of n=1 2D HPs with conventional spacers (e.g., butylammonum (BA), phenethylammonium (PEA) and so on; ~520 nm)[2, 15]. Such deviations and PL asymmetry can be attributed to the substantial Pb^{2+} off-center displacement, as a consequence of severe $[PbI_6]^{4-}$ octahedral distortion driven by the compact packing of bulky DPA cation[7]. To compensate for the lattice distortion, the lone pair of Pb^{2+} ($6s^2$) can be geometrically localized in the octahedra, which thereby leads to appreciable changes in band-edge states. The electronic density of states determined by DFT for the $DPA_{1.5}Cs_{0.5}PbI_4$ lattice (i.e., 75% DPA coverage) exhibits a larger bandgap by 0.45 eV compared with Cs_2PbI_4 lattice (**Figure 2g and h**). Considering the inappreciable impact of A-site cation itself on the frontier energy level landscape of HPs[6, 17], the predicted large bandgap widening also corroborates that structural distortion by the compact packing of DPA is a major attribute for the PL blueshifts in n=1 DPA_2PbI_4.

Further increases of 3D $APbI_3$ ratios produce darker, brown, or black film crystallites, involving new PL peaks at a higher wavelength range (i.e., centered at 600-800 nm; **Figure S1**). Specifically, these peaks redshift with increasing 3D $APbI_3$ ratios, at the expense of the asymmetric PL peaked at 490 nm. This indicates the formation of quasi-2D HPs with thick inorganic layers or 3D-like HPs where more A-site cation can be incorporated into the lattice, while the formation of n=1 2D HP structure is less favored[2, 15, 19]. At high 3D $APbI_3$ ratios, except for the case of $MAPbI_3$ incorporation, pale-yellow crystallites are formed. This is attributed to the formation of thermodynamically feasible, non-perovskite δ-$CsPbI_3$ or δ-$FAPbI_3$ phases (for the binary system with $CsPbI_3$ and $FAPbI_3$ endmembers, respectively) at the low annealing temperature (<100 $^{\circ}$C).

To understand the crystallographic structures in these 2D-3D binary HP compositional spaces, X-ray diffraction (XRD) patterns of the synthesized films with different 3D composition ratios in each system were collected (**Figure S2**). As predicted from absorption and PL features, 100% stoichiometric DPA_2PbI_4 exhibits no appreciable diffraction peaks due to the unfeasible crystallization. At low 3D concentrations (5%, 6%, and 4% of $CsPbI_3$, $MAPbI_3$, and $FAPbI_3$, respectively), distinctive XRD peak series at 4.26° 8.47°, and 12.69° (marked with yellow diamonds) appear – particularly for Cs- and MA-based systems, where the corresponding patterns are respectively shown in **Figure 2i**. The corresponding d-spacing

calculated from the XRD peaks (i.e., 2.07 nm) is qualitatively coincidence with the possible interlayer distances between the neighboring DPA_2PbI_4 sheets in an optimized $CsPbI_3$-based DFT model structure (~2.083 nm; **Figure S3**), and thus we assign these XRD patterns to the (00n) periodic stacking modes of n=1 2D DPA_2PbI_4 HPs[2, 19].

Note that, for the case of $FAPbI_3$ incorporation, the emergence of (002) diffraction peak is weaker than those in $CsPbI_3$ or $FAPbI_3$-incorporated system. Given the larger effective ionic radii of FA compared with Cs and MA[25], presumably, sufficient regulation on the magnitude of octahedral distortion can be achieved with relatively smaller amounts of FA incorporation. In turn, this can also promote the emergence of a quasi-2D HP structure at a relatively smaller $FAPbI_3$ ratio than Cs- and MA-counterparts. Further increasing 3D concentrations results in the multiple emergence of new peaks – particularly at ~3.86°, 4.53°, and 4.97°, likely associated with the formation of quasi-2D HP structures (i.e., n≥2 2D). Also, at high 3D ratios, the XRD patterns of bulk 3D HP (case of $MAPbI_3$) or δ-phases (cases of $CsPbI_3$ and $FAPbI_3$) were observed.

Overall, both computational and high-throughput experimental results collectively suggest that the synthesis of n=1 2D DPA_2PbI_4 is indeed feasible only when minor fractions of $APbI_3$ – qualitatively irrespective of the exact species of A-site cation – are delicately incorporated. Raman scattering analysis on the synthesized DPA_2PbI_4 films further reveals the emergence of multiple peaks irrespective of the selection of A-site cation, which is not observed in PbI_2 (**Figure S4**)[7, 26]. The change in lattice modes at low wavenumbers and slight shifting of numerous organic ligand modes, as compared to those of neat DPAI crystallites, is plausibly due to the lattice interactions of the synthesized film crystallites consisting of DPA cations. Thus, the observation further justifies that the products are indeed crystalline 2D DPA_2PbI_4 films. Note that the construction of 2D HPs with sole exploitation of sterically hindered spacer cation has not been considered so far. In addition, the concept of $APbI_3$ incorporation for the synthesis of 2D HP is, essentially, beyond the classical chemical intuition. These collectively indicate that the realization of 2D DPA_2PbI_4 structure, and its chemical requisites, could only be achieved by implementation of the high-throughput autonomous, combinatorial exploration workflow.
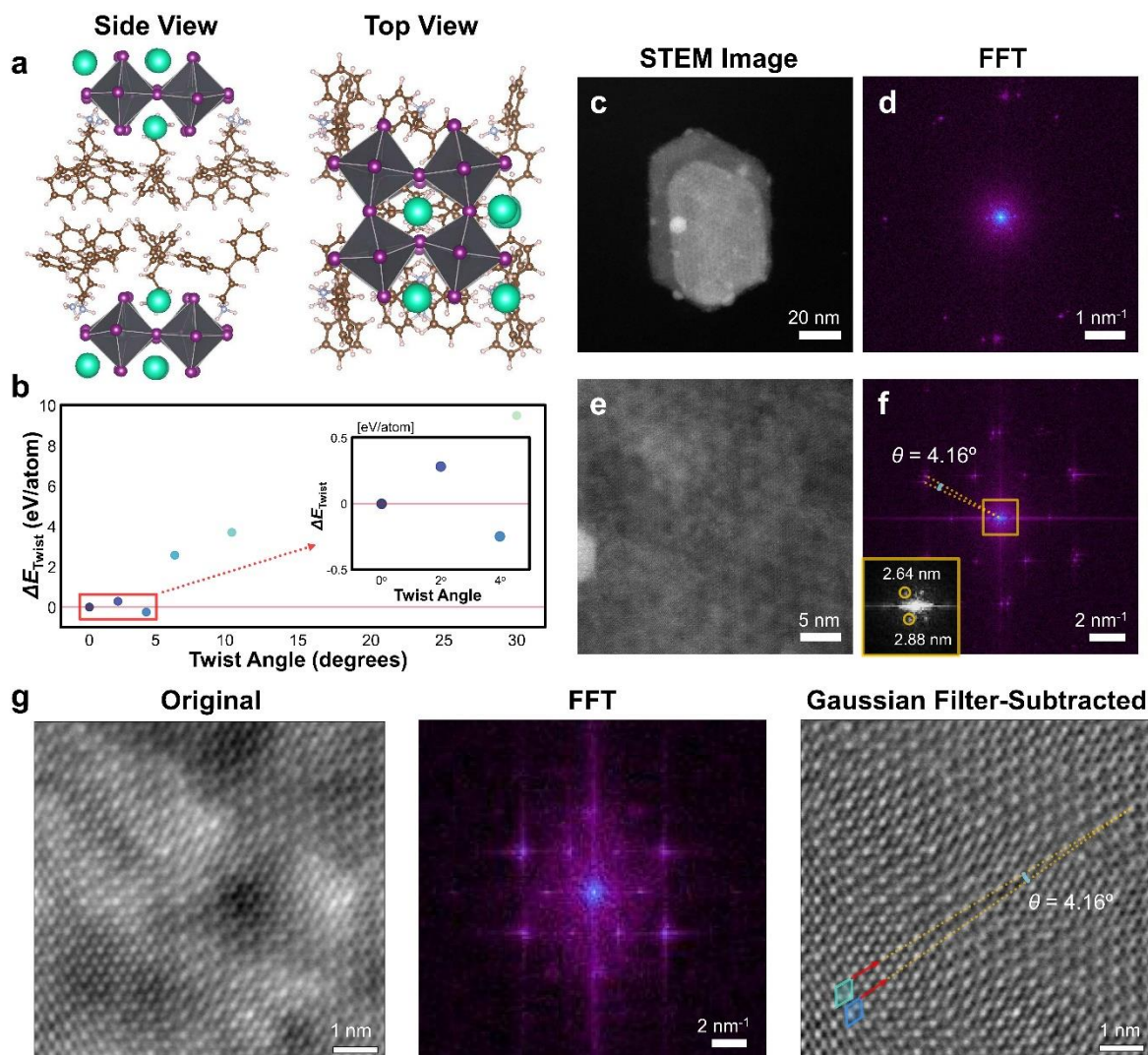
Figure 3. (**a**) Side and top views of an optimized 2D HP stack structure where DPA-coordinated sides (75% DPA coverage) are facing each other. (**b**) Calculated energy stabilization of the 2D HP layer stack system at different twist angles. (**c,e**) Low- and high-magnification HAADF-STEM images of the DPA_2PbI_4 stacking flake and (**d,f**) the corresponding FFT patterns, respectively. (**g**) High-resolution HAADF-STEM atomic structure (left), FFT pattern (middle), and Gaussian filter-subtracted image from the original (right) atomic structure of DPA_2PbI_4 surface.

Observation of self-assembled twisted stack in DPA-based 2D HPs

For 2D HPs based on conventional spacer cations with aromatic rings (e.g., PEA_2PbI_4), the coordinated spacers render an ordered alignment on the 2D HP surface, presumably offering an electrostatically planar surface that manifests coherent stacking orientation upon the layer stacking. Reportedly, those 2D HP sheets are epitaxially stacked across the crystallites[27]. In contrast, for DPA_2PbI_4 2D HP, the compact alignment of bulky DPA – particularly its two phenyl rings, can offer a flexible and disordered van der Waals surface (**Figure S5**). Encouraged by this extraordinary surface electrostatic feature, we hypothesize that DPA_2PbI_4 can manifest

9

the self-assembly of an additional 2D HP layer in a twisted stack.

We first constructed a bilayer stack of DPA_2PbI_4 2D sheets where the DPA-coordinated 2D HP surfaces (75% coverage) are facing each other (**Figure 3a**), and calculated the DFT energy differences of the system at different twist angles with respect to the untwisted counterpart (ΔE_{Twist}; **Figure 3b**). Overall, the trend of ΔE_{Twist} exhibits a monotonic increase with increasing the twist angle up to 30°, except for the case at 4° showing a negative value. These simulated results indicate that 4° of twisted assembly is more favored than the epitaxial assembly scenario upon the construction of 2D DPA_2PbI_4 HP stack.

To obtain atomic-scale insight into the twisted stacking behaviors of DPA_2PbI_4 HPs, scanning transmission electron microscopy (STEM) images of the stacked HP flakes were collected. Here, we prepared the HP flakes by coercing crystallization of the precursor solutions directly drop-casted on the TEM grid via antisolvent immersion. This allows for the production of DPA-incorporated HP crystallites irrespective of the selection of 3D endmembers, as confirmed via electron energy loss spectroscopy (EELS) (**Figure S6**). Representatively, we explored the MA-based precursor mixture due to the thermodynamic feasibility in HP crystallization as confirmed by XRD analysis.

In both low- and high-magnification high-angle annular dark field (HAADF) views (**Figure 3c and e**), a periodic array of circular and dark motifs appeared on the 2D HP surface, clearly showing the establishment of Moiré superlattices by the twisted HP stacks. Corresponding the fast Fourier-transform (FFT) patterns also reveal the twisted alignment of the diffraction spot with an average angle of ~4.16° as well as the Moiré spots with a *d*-spacing of ~2.7 nm (**Figure 3d and f**), strongly consistent with theoretical prediction. The high-resolution HAADF-STEM image of the DPA_2PbI_4 HP surface, after subtracting Gaussian filtered image, also clearly shows the ~4°-twisted alignments of atomic structures oriented from each 2D HP layer sheet (**Figure 3g**), for the first time to the best of our knowledge.

Collectively, these findings suggest that the unique alignment of the bulky DPA spacer cation, as well as the unconventional landscape of van der Waals surface of DPA_2PbI_4 can indeed manifest twisted 2D HP stacks. Specifically, the construction of the twisted 2D HP stack occurs spontaneously, indicating the stacking behaviors are driven by the self-assembly action during crystallization. Note that such a straightforward, bottom-up approach of twisted stacking in 2D HP has not been demonstrated in other 2D materials systems; manifesting such unconventional structure requires meticulous experimental procedures and controls, as well as extensive costs and laborious efforts[3, 4, 24]. This emphasizes a new opportunity in 2D HPs with bulky spacers where the delicate chemical manipulations of the twisted stacking are feasible and thus, we believe that this approach opens a new avenue to explore a new exotic materials systems and functionalities.

Outlook

In summary, through high-throughput first principles simulations and experimental exploration, we have revealed that DPA can act as a spacer cation for 2D HPs, which has been rarely considered due to its bulky molecular structure attributed to two phenyl rings. We confirmed that the minute incorporation of 3D $APbI_3$ endmember precursor allows for the synthesis of *n*=1 2D DPA_2PbI_4 HP structure by mitigating the steric hindrance between the

neighboring DPA cations in their compact packing on 2D HP surface. It should be noted that such an extraordinary, off-stoichiometric strategy for 2D HP synthesis has not been previously considered, essentially due to the difficulty of envisaging based on conventional intuition in perovskite chemistry. In this regard, we emphasize that high-throughput combinatorial explorations was perhaps the only way to realize such unconventional materials and chemistry discoveries.

In addition, with excellent agreement between theoretical and experimental observations, we have shown that the compact packing of DPA spacer cations on 2D HP surface can manifest self-assembly of twisted 2D HP layer stacks, which has not been observed from conventional 2D HP systems with linear spacers. Our observations – as a result of delicate supramolecular interactions along the spacer ligand system – open a new avenue to manipulate twisted 2D HP structures. Specifically, comprehensive exploration of the chemistry of organic molecular spacers in the DPA structural framework – engineering of functional groups, stereochemistry, and so on – can elucidate delicate design principles that 'chemically' manipulate the twist angles of the 2D HP stacks. Note that, the twisted stacks demonstrated in other 2D materials have been realized via a top-down approach requiring meticulous experimental procedures and extensive efforts[3, 4, 24]. In contrast, the twisted stacking behaviors of DPA-based 2D HP are essentially driven by the self-assembly of building blocks during crystallization, where the synthetic procedure is much straightforward and cost-effective. Given the intriguing and unconventional excitonic and electronic features in Moiré superlattices based on other 2D materials systems, which are, however, rarely reported in promising HP materials systems, our finding are a milestone for initiating and accelerating bottom-up exploration of new functionalities and fundamental principles in versatile 2D HPs.

Methods

Ab Initio Calculations

DFT calculatiions were carried out using the Vienna *Ab-Initio* Software Package (VASP)[28, 29]. Lattice constants for bulk $CsPbI_3$ were determined using the Perdew-Burke Ernzerhof (PBE) functional with a 350 eV electronic energy cutoff and a 6x6x6 Γ-centered K-Point mesh. The self-consistent field energy convergence criteria was set to 1×10^{-6} eV, and the force criteria for the ionic steps was set to 0.01 eV/Å. $CsPbI_3$ and Cs_2PbI_4 monolayers were constructed from the optimized bulk structure, incorporating a 20 Å vacuum space perpendicular to the monolayers along the c-axis to prevent spurious interactons. To accomadate the excessive number of atoms in some of the monolayer and bilayer calculations (> 200 atoms), the convergence criteria was adjusted to 1×10^{-5} eV and 0.02 eV/Å for the energy and force calculations, respectively. Additionally, the Γ-centered KPOINT grid was reduced to 2x2x1. The binding energies for DPA binding were calculated using the $CsPbI_3$ monolayers, which allowed for us to study steric hindrance by substituting Cs atoms only on the top layer of the structure (equation 1):

$$\Delta E_b(n) = E_{CsPbI_3,DPA} + nE_{Cs} - \left(E_{CsPbI_3} + nE_{DPA} \right) \text{ (equation 2)}$$

where $E_{CsPbI_3,DPA}$ is the total energy of the $CsPbI_3$ and DPA complex, E_{CsPbI_3} and E_{DPA} are the total energies for isolated $CsPbI_3$ monolayers and DPA molecules, E_{Cs} is the energy per atom

11

of bulk Cs, and n represents the number of Cs vacancies or DPA molecules (assumed equal here). Monolayer electronic structure calculations used the Cs_2PbI_4 geometry, which allowed for DPA substitution on both sides of the monolayer. The density of states (DOS) were calculated for both a pure Cs_2PbI_4 monolayer, and a monolayer with 75% DPA substitution. The geometries for these structures were optimized using the same procedure as described for $CsPbI_3$ monolayers. However, the DOS were calculated using the HSE06 functional[30]. Twisted bilayers were constructed from the optimized geometry of the $CsPbI_3$ monolayers with 75% DPA, and the stability of different bilayer twist angles were determined using the same geometry optimization conditions described for monolayers. The interlayer spacing for the most stable twist angle (4°) was also calculated using the Cs_2PbI_4 geometry for comparison, and showed little difference between the two geometries (~0.04 nm).

High-throughput synthesis

DPAI salts were synthesized by mixing DPA and HI in ethanol and subsequent recrystallization with diethyl ether, according to a protocol in the literature[18]. 0.5 M of 2D DPA_2PbI_4 and 3D $APbI_3$ precursors in DMF:DMSO solution (9:1) were prepared by dissolving stoichiometric amounts of materials in an N_2 glove box. Those endmember solutions were stirred overnight at room temperature. Then the solutions were transferred to a pipetting robot platform (Opentrons, OT-2) in the N_2 atmosphere.

The overall experimental setup for a high-throughput robotic synthesis platform is done according to our previous reports[2, 19, 20, 22]. By using a 300 μL-capacity single-channel pipet, 50 μL of quasi-2D precursor solutions with a targeted 2D:3D ratio, are filled in each well of a microplate. Then, by using a 20 μL-capacity 8-channel pipet, 0.5 μL of the prepared solutions were dispensed onto the UV/O_3-treated glass substrates placed on the heating module with a fixed temperature of 95 °C. The droplets are crystallized at 95 °C for 10 min.

Characterization

XRD patterns of the quasi-2D HP films were collected by using X-ray diffractometer (Empyrean; Malvern Panalytical). Raman spectra were collected by using a Horiba XploRA PLUS system with a 785 nm laser focused through a 100× objective lens.

STEM

Scanning transmission electron microscopy was performed on a Nion UltraSTEM100 operated at 60 kV with a semiconvergence angle of 32 mrad. To minimize carbon contamination, the specimens were baked in high vacuum conditions to 80 °C overnight prior to loading into the microscope. HAADF-STEM imaging was performed with a nominal probe current of 30 pA, with a scattering collection semiangle from 80-200 mrad. To mitigate beam-induced transformations, electron exposure was kept to a minimum by using short pixel dwell times (11 us) and the beam was blanked between image acquisition and navigation. Core loss STEM-EELS was performed using an Enfina spectrometer with 0.5 eV/ch and pixel dwell times of 0.5s. The samples were directly crystallized on the TEM grid (with carbon formvar). Briefly, TEM grids are placed on a hot plate and the heated to 95 °C. At this temperature, 10 μL of Toluene (as an antisolvent) was drop-casted onto the TEM grid, and then precursor solutions

(diluted to 0.1 M) were quickly dropped onto the wet grid. The resulting specimens were annealed at 95 °C for 10 min.

Acknowledgements

References

(1) Li, X. T.; Hoffman, J. M.; Kanatzidis, M. G. The 2D Halide Perovskite Rulebook: How the Spacer Influences Everything from the Structure to Optoelectronic Device Efficiency. *Chem Rev* **2021**, *121* (4), 2230-2291. DOI: 10.1021/acs.chemrev.0c01006.

(2) Yang, J.; Lawrie, B. J.; Kalinin, S. V.; Ahmadi, M. High-Throughput Automated Exploration of Phase Growth Behaviors in Quasi-2D Formamidinium Metal Halide Perovskites. *Adv Energy Mater* **2023**, 2302337.

(3) Choi, S. H.; Yun, S. J.; Won, Y. S.; Oh, C. S.; Kim, S. M.; Kim, K. K.; Lee, Y. H. Large-scale synthesis of graphene and other 2D materials towards industrialization. *Nat Commun* **2022**, *13* (1), 1484. DOI: 10.1038/s41467-022-29182-y.

(4) Mannix, A. J.; Kiraly, B.; Hersam, M. C.; Guisinger, N. P. Synthesis and chemistry of elemental 2D materials. *Nat Rev Chem* **2017**, *1*, 0014.

(5) Zhao, X.; Ball, M. L.; Kakekhani, A.; Liu, T.; Rappe, A. M.; Loo, Y. L. A charge transfer framework that describes supramolecular interactions governing structure and properties of 2D perovskites. *Nat Commun* **2022**, *13*, 3970.

(6) Shao, Y.; Gao, W.; Yan, H.; Li, R.; Abdelwahab, I.; Chi, X.; Rogee, L.; Zhuang, L.; Fu, W.; Lau, S. P.; et al. Unlocking surface octahedral tilt in two-dimensional Ruddlesden-Popper perovskites. *Nat Commun* **2022**, *13* (1), 138. DOI: 10.1038/s41467-021-27747-x.

(7) Gu, J.; Tao, Y.; Fu, T.; Guo, S.; Jiang, X.; Guan, Y.; Li, X.; Li, C.; Lu, X.; Fu, Y. Correlating Photophysical Properties with Stereochemical Expression of $6s^2$ Lone Pairs in Two-dimensional Lead Halide Perovskites. *Angew Chem Int Ed* **2023**, *62* (30), e202304515. DOI: 10.1002/anie.202304515.

(8) Gao, Y.; Shi, E.; Deng, S.; Shiring, S. B.; Snaider, J. M.; Liang, C.; Yuan, B.; Song, R.; Janke, S. M.; Liebman-Pelaez, A.; et al. Molecular engineering of organic-inorganic hybrid perovskites quantum wells. *Nat Chem* **2019**, *11* (12), 1151-1157. DOI: 10.1038/s41557-019-0354-2.

(9) Shi, E.; Yuan, B.; Shiring, S. B.; Gao, Y.; Akriti; Guo, Y.; Su, C.; Lai, M.; Yang, P.; Kong, J.; et al. Two-dimensional halide perovskite lateral epitaxial heterostructures. *Nature* **2020**, *580* (7805), 614-620. DOI: 10.1038/s41586-020-2219-7.

(10) Wang, K.; Lin, Z. Y.; Zhang, Z.; Jin, L.; Ma, K.; Coffey, A. H.; Atapattu, H. R.; Gao, Y.; Park, J. Y.; Wei, Z.; et al. Suppressing phase disproportionation in quasi-2D perovskite light-emitting diodes. *Nat Commun* **2023**, *14* (1), 397. DOI: 10.1038/s41467-023-36118-7.

(11) Park, J. Y.; Song, R.; Liang, J.; Jin, L.; Wang, K.; Li, S.; Shi, E.; Gao, Y.; Zeller, M.; Teat, S. J.; et al. Thickness control of organic semiconductor-incorporated perovskites. *Nat Chem* **2023**, *15* (12), 1745-1753. DOI: 10.1038/s41557-023-01311-0.

(12) Yang, J.; Kalinin, S. V.; Cubuk, E. D.; Ziatdinov, M.; Ahmadi, M. Toward self-organizing low-dimensional organic–inorganic hybrid perovskites: Machine learning-driven co-navigation of chemical and compositional spaces. *MRS Bull* **2023**, *48*, 164-172.

(13) Arciniegas, M. P.; Manna, L. Designing Ruddlesden–Popper Layered Perovskites through Their Organic Cations. *ACS Energy Lett* **2022**, *7*, 2944-2953.

(14) Passarelli, J. V.; Fairfield, D. J.; Sather, N. A.; Hendricks, M. P.; Sai, H.; Stern, C. L.; Stupp, S. I. Enhanced Out-of-Plane Conductivity and Photovoltaic Performance in n = 1 Layered Perovskites through Organic Cation Design. *J Am Chem Soc* **2018**, *140*, 7313-7323.

(15) Zhang, J.; Wu, J.; Langner, S.; Zhao, B.; Xie, Z.; Hauch, J. A.; Afify, H. A.; Barabash, A.; Luo, J.; Sytnyk, M.; et al. Exploring the Steric Hindrance of Alkylammonium Cations in the Structural Reconfiguration of Quasi-2D Perovskite Materials Using a High-throughput Experimental Platform. *Adv Funct Mater* **2022**, *32*, 2207101.

(16) Mao, L.; Wu, Y.; Stoumpos, C. C.; Wasielewski, M. R.; Kanatzidis, M. G. White-Light Emission and Structural Distortion in New Corrugated Two-Dimensional Lead Bromide Perovskites. *J Am Chem Soc* **2017**, *139* (14), 5210-5215. DOI: 10.1021/jacs.7b01312.

(17) Tang, G.; Ghosez, P.; Hong, J. Band-Edge Orbital Engineering of Perovskite Semiconductors for Optoelectronic Applications. *J Phys Chem Lett* **2021**, *12* (17), 4227-4239. DOI: 10.1021/acs.jpclett.0c03816.

(18) Song, H.; Yang, J.; Jeong, W. H.; Lee, J.; Lee, T. H.; Yoon, J. W.; Lee, H.; Ramadan, A. J.; Oliver, R. D. J.; Cho, S. C.; et al. A Universal Perovskite Nanocrystal Ink for High-Performance Optoelectronic Devices. *Adv Mater* **2023**, *35* (8), e2209486. DOI: 10.1002/adma.202209486.

(19) Yang, J.; Hidalgo, J.; Song, D.; Kalinin, S. V.; Correa-Baena, J. P.; Ahmadi, M. Accelerating materials discovery by high-throughput GIWAXS characterization of quasi-2D formamidinium metal halide perovskites. *ChemRxiv* **2023**, 10.26434/chemrxiv-22023-x26437sfr-v26433.

(20) Foadian, E.; Yang, J.; Tang, Y.; Harris, S. B.; Rouleau, C. M.; Joy, S.; Graham, K. R.; Lawrie, B. J.; Hu, B.; Ahmadi, M. Decoding the Broadband Emission of Two-Dimensional Pb-Sn Halide Perovskites through High-Throughput Exploration. *ChemRxiv* **2023**, 10.26434/chemrxiv-22023-wttkj.

(21) Higgins, K.; Ziatdinov, M.; Kalinin, S. V.; Ahmadi, M. High-Throughput Study of Antisolvents on the Stability of Multicomponent Metal Halide Perovskites through Robotics-Based Synthesis and Machine Learning Approaches. *J Am Chem Soc* **2021**, *143* (47), 19945-19955. DOI: 10.1021/jacs.1c10045.

(22) Sanchez, S. L.; Tang, Y. P.; Hu, B.; Yang, J.; Ahmadi, M. Understanding the ligand-assisted reprecipitation of CsPbBr3 nanocrystals via high-throughput robotic synthesis

approach. *Matter-Us* **2023**, *6* (9), 2900-2918. DOI: 10.1016/j.matt.2023.05.023.

(23) Blancon, J. C.; Even, J.; Stoumpos, C. C.; Kanatzidis, M. G.; Mohite, A. D. Semiconductor physics of organic-inorganic 2D halide perovskites. *Nat Nanotechnol* **2020**, *15* (12), 969-985. DOI: 10.1038/s41565-020-00811-1.

(24) Zhang, S.; Jin, L.; Lu, Y.; Zhang, L.; Yang, J.; Zhao, Q.; Sun, D.; Thompson, J. J. P.; Yuan, B.; Ma, K.; et al. Square Moiré Superlattices in Twisted Two-Dimensional Halide Perovskites. *arXiv* **2023**, DOI:10.48550/arXiv.42312.16679.

(25) Lee, J. W.; Tan, S.; Seok, S. I.; Yang, Y.; Park, N. G. Rethinking the A cation in halide perovskites. *Science* **2022**, *375* (6583), eabj1186. DOI: 10.1126/science.abj1186.

(26) Pérez-Osorio, M. A.; Lin, Q.; Phillips, R. T.; Milot, R. L.; Herz, L. M.; Johnston, M. B.; F., G. Raman Spectrum of the Organic–Inorganic Halide Perovskite CH3NH3PbI3 from First Principles and High-Resolution Low-Temperature Raman Measurements. *J Phys Chem C* **2018**, *122*, 21703-21717.

(27) Sheikh, M. A. K.; Kowal, D.; Mahyuddin, M. H.; Cala, R.; Auffray, E.; Witkowski, M. E.; Makowski, M.; Drozdowski, W.; Wang, H.; Dujardin, C.; et al. $A_2B_{n-1}Pb_nI_{3n+1}$ (A = BA, PEA; B = MA; n = 1, 2): Engineering Quantum-Well Crystals for High Mass Density and Fast Scintillators. *J Phys Chem C* **2023**, *127* (22), 10737-10747.

(28) Kresse, G.; Furthmüller, J. Efficiency of ab-initio total energy calculations for metals and semiconductors using a plane-wave basis set. *Comput Mater Sci* **1996**, *6*, 15-50.

(29) Kresse, G.; Furthmüller, J. Efficient iterative schemes for ab initio total-energy calculations using a plane-wave basis set. *Phys Rev B Condens Matter* **1996**, *54* (16), 11169-11186. DOI: 10.1103/physrevb.54.11169.

(30) Heyd, J.; Scuseria, G. E.; Ernzerhof, M. Hybrid functionals based on a screened Coulomb potential. *J Chem Phys* **2003**, *118*, 8207.